

Document downloaded from:

<http://hdl.handle.net/10251/74560>

This paper must be cited as:

Desantes J.M.; Salvador Rubio, FJ.; López, JJ.; De La Morena, J. (2011). Study of mass and momentum transfer in diesel sprays base on X-ray mass distribution measurements and on a theoretical derivation. *Experiments in Fluids*. 50(2):233-246. doi:10.1007/s00348-010-0919-8.



The final publication is available at

<http://dx.doi.org/10.1007/s00348-010-0919-8>

Copyright Springer Verlag (Germany)

Additional Information

# **STUDY OF MASS AND MOMENTUM TRANSFER IN DIESEL SPRAYS BASED ON X- RAY MASS DISTRIBUTION MEASUREMENTS AND ON A THEORETICAL DERIVATION.**

J.M. Desantes, F.J. Salvador (\*), J.J. López, J. De la Morena.

*CMT-Motores Térmicos, Universidad Politécnica de Valencia, Camino de Vera  
s/n, E-46022 Valencia, Spain*

(\*). Corresponding author:

Dr. Francisco Javier Salvador

Telephone: +34-963879658

FAX: +34-963877659

[fsalvado@mot.upv.es](mailto:fsalvado@mot.upv.es)

In this paper a research aimed at quantifying mass and momentum transfer in the near-nozzle field of diesel sprays injected into stagnant ambient air is reported. The study combines x-ray measurements for two different nozzles and axial positions, which provide mass distributions in the spray, with a theoretical model based on momentum flux conservation which was previously validated. This investigation has allowed the validation of Gaussian profiles for local fuel concentration and velocity near the nozzle exit, as well as the determination of Schmidt number at realistic diesel spray conditions. This information could be very useful for those who are interested in spray modelling, especially at high pressure injection conditions.

*Keywords: Diesel sprays, near field, Schmidt number, concentration, modelling, x-ray*

## List of symbols

$A$	Outlet hole section.
$C(x,r)$	Local spray mass concentration.
$C_v(x,r)$	Local spray volume concentration.
$C_{axis}(x)$	Concentration at a determined axial position of the spray.
$D$	Mass diffusivity.
$I$	X-ray beam intensity after passing through the spray.
$I_0$	X-ray beam incident intensity.
$i$	Counter of Taylor's series.
$j$	Counter used in the determination of the Mean Squared Deviation (MSD) between PDPA data and prediction by radial profiles.
$k$	Constant used in fitted Gaussian profiles.
$M'$	Projected mass obtained from x-ray measurements.
$\dot{M}_o$	Momentum flux at the nozzle orifice outlet.
$m_a$	Air mass.
$m_f$	Fuel mass.
$\dot{m}_f$	Fuel mass flow rate.
$MSD$	Mean Squared Deviation between PDPA experiments and theoretical radial profiles.
$p, q$	Counters in the numerical procedure for determining the optimal Schmidt number.
$N$	Number of terms in the Taylor series.
$n_r$	Number of measuring points in the radial direction.
$n_x$	Number of measuring points in the axial direction.
$n_{ex}$	Number of measurements from PDPA.
$P_{back}$	Backpressure.
$P_{in}$	Injection pressure.

$r$	Radial coordinate.
$r_l$	Radial position of the x-ray beam at the central plane of the spray.
$r_{1/2}$	Radial position at which local spray velocity decreases until a value of $0.5 \cdot U_{axis}$ .
$R$	Radius of the spray defined from velocity profile.
$R_m$	Radius of the spray defined from concentration profile.
$S$	Spray tip penetration.
$Sc$	Schmidt Number.
$t$	Time from the start of injection.
$U_{axis}(x)$	Velocity at the spray's axis.
$U_o$	Orifice outlet velocity.
$U(x, r)$	Local spray velocity.
$U_{ex}(x_j, r_j)$	Experimental local velocity value from PDPA measurements at experiment $j$ .
$U_{mo}(x_j, r_j)$	Local velocity value estimated from a theoretical radial profile at experiment $j$ .
$V_a$	Local volume occupied by air.
$V_f$	Local volume occupied by fuel.
$x$	Axial coordinate.
$z$	Axial perpendicular coordinate used in the experimental x-ray measurements.

## Greek symbols:

$\alpha$	Coefficient of the Gaussian radial profile for the axial velocity.
$\varepsilon$	Mean deviation in the prediction of $M'$ .
$\phi_{eq}$	Equivalent diameter.
$\phi_o$	Outlet diameter of the nozzle's orifice.
$\rho$	Local spray density defined as $\rho = \frac{m_a + m_f}{V_a + V_f}$ .

$\rho_L$	Local fuel density defined as $\rho_L = \frac{m_f}{V_a + V_f}$ .
$\rho_a$	Ambient density.
$\rho_f$	Fuel density.
$\nu$	Kinematic viscosity.
$\pi$	Pi number.
$\theta_m$	Spray cone angle defined from mass distribution.
$\theta_u$	Spray cone angle defined from velocity distribution.

# 1. Introduction

Despite being used in many industrial applications, the study of sprays has always been difficult due to the complex phenomena involved: atomization, mixing, coalescence, transfer of mass and momentum and evaporation (Lefèbvre 1989, Dumouchel 2008). This complexity is accentuated when studying sprays in direct injection diesel engines because of the high frequency transient operation and the small characteristic injection time and length (~1 ms and 25 mm). In such adverse conditions from the point of view of experimentation, the spray characteristics that can be measured are quite limited, especially in the densest part of the spray (near-nozzle region). The most typical characteristics are spray tip penetration and spray cone angle (Hiroyasu and Arai 1990; Naber and Siebers 1996; Way 1997; Roisman *et al.* 2007), which are macroscopic characteristics, and droplet velocity and droplet diameter, which are microscopic features (Wu *et al.* 1986; Jawad *et al.* 1992; Roisman and Tropea 2001; Subramaniam 2001). Nevertheless, in the studies available in the literature, the microscopic features are normally measured for axial positions far from the nozzle orifice, where local density in the spray has decreased due to air entrainment. This is especially true when the characterization is made by means of Phase Doppler Particle Analyzer systems (PDPA), which cannot work properly if droplet concentration is higher than a given threshold. In the last years, new and original techniques have been developed, helping to get further information about spray structure. As an example, x-ray measurements have shown to be useful in order to obtain information about mass distribution in the dense primary break-up (Leick *et al.* 2007; Tanner *et al.* 2006; Ramirez *et al.* 2009). As a consequence, in some cases, microscopic measurements are becoming as reliable as macroscopic ones, so that the relationship existing between them can be properly studied.

One of the key parameters that relate microscopic and macroscopic characteristics of the spray is momentum flux. It is considered by several authors as one of the most important parameters governing the spray dynamics (Way 1997; Cossali 2001, Payri, F. *et al.* 2004; Desantes *et al.* 2006a). Momentum flux is a direct function of effective flux velocity at the orifice outlet, fuel density and effective diameter of the nozzle orifice and it can be properly measured using a suitable methodology (Payri, R. *et al.* 2005).

As evidence of the importance of momentum flux on spray dynamics, Ricou and Spalding (1961) found out that different gas jets behave in a similar way if both momentum flux and exit velocity are the same. Additionally, and as a result of a theoretical approach based on momentum flux conservation along the spray axis, a mathematical model was derived by Desantes *et al.* (2007) in which the momentum flux was related with the axial profiles of velocity and concentration. The main contribution of the model with respect to previous work in the literature (Dent 1971; Naber and Siebers 1996; Correas 1998) was the consideration of local density variations and the deduction of the model for a generic Schmidt number. Despite the relevance of the Schmidt number, which represents the relative rate of momentum and mass transfer in the spray, contributions about its value are quite scarce in sprays specialized literature on sprays. Only Prasad and Kar (1976) gave a range of value of 0.7-0.8, using an injection pressure of 10-20 MPa and nozzle diameters between 0.4 and 0.57 mm. These values seemed to be dependent on injection pressure since a lower value was obtained at an injection pressure of 20 MPa. Nevertheless, injection parameters were quite far from current diesel injection conditions, both in terms of injection pressures and nozzle diameters. Despite having shown theoretically that the influence of Schmidt number on concentration and velocity profiles is mainly important in the near nozzle field, the model proposed by Desantes *et al.* (2007) has only been validated in the past by means of velocity measurements using a PDPA system and for axial distances no smaller than 25 mm, due to requirements of measurement principle. Thus, although the experimental characterization was useful to provide reliability to the model derived, nothing could be concluded about actual values of the Schmidt number in real high pressure applications. In this paper, thanks to an innovative technique based on x-ray radiography developed at Argonne National Laboratories (Leick *et al.* 2007, Tanner *et al.* 2006), valuable information has been obtained and processed with the aim of consolidating the validity of the model and, furthermore, in order to obtain an estimated value for the Schmidt number.

As far as the structure of the paper is concerned, the article is divided in 4 parts. In section 2, the basis of the model is summarized accompanied by an example of the complete validation against PDPA measurements that was made in the past and published in Desantes *et al.* (2007) and Payri, R. *et al.* (2008). In section 3,

raw measurements provided from x-ray technique are given, as well as the way they have been processed and combined with the model in order to obtain the maximum possible information. Analysis of results of two different nozzles is performed in this section where, as a main result of the investigation, an approximation of the Schmidt number value under typical diesel sprays conditions is given. Finally, in section 4, the most important conclusions of the work are drawn.

## 2. Spray dynamics

### 2.1. Background

The structure of diesel sprays has been widely studied over the last decades. The atomization process in a spray is a complex phenomenon, which is strongly affected by different aspects such as cavitation or turbulence inside the nozzle (Reitz and Bracco 1982; Payri, F. *et al.* 2004; Dumouchel 2008). Traditionally, the internal structure of the steady zone of the spray has been divided into two regions: the initial region, located near the orifice of the nozzle, where fuel concentration along the spray axis can be considered as equal to the unity, and the local velocity is still the same as the exit velocity, and the main or fully developed region, where the fuel in the whole section of the spray includes a significant air fraction (Hiroyasu and Arai 1990). A schematic view of these two regions is presented in Fig 1. More recently, other studies (Yue *et al.* 2001) have pointed out that spray could be actually disrupted immediately after leaving the nozzle due to the characteristics of internal nozzle flow. Nevertheless, the present theoretical development will focus on the main steady region of the spray, once primary break-up has been undergone.

Many advances have been made in the fluid mechanics of single-phase jets in the past, and the quantitative and qualitative basis established for the jet theory can be conveniently utilized for the spray phenomenon as well. Adler and Lyn (1969) proposed a study of sprays using a continuous model of a gas jet, stating that this was justified due to the similarity between gas jets and sprays from the point of view of basic mechanisms. Since then, many other researchers have followed this path, as for example Rife and Heywood (1974), who developed a model to predict spray behaviour based on the gas jet equation, or Prasad and Kar (1976), who



performed an investigation in order to analyse the processes of diffusion of mass and velocity, obtaining quantitative data for treating the diesel spray as a turbulent jet. These and many other investigations imply that many results from the literature concerning gas jets can be directly applicable to sprays. The main difference between a turbulent gas jet and a spray is that, for a given nozzle geometry, the jet has a constant cone angle (Spalding 1979) which depends neither on injection pressure nor on ambient density, whilst the diesel spray has a cone angle that depends on the operating conditions (Wu *et al.* 1984; Coghe and Cossali 1994; Way 1997; Payri, R. *et al.* 2005) or indirectly on the presence or not of cavitation (Payri, F. *et al.* 2004; Sou *et al.* 2007). In this statement, the cone angle is assumed to be the one corresponding to the main region of the jet or spray (see Figure 1). An additional important feature concerning the radial evolution of axial velocity and fuel concentration is self-similarity. Rajaratnam (1976), among others (Abramovich 1963; Hinze 1975; Sinnamon *et al.* 1980; Lefèbvre 1989; Desantes *et al.* 2006b), found that, for any section in the fully developed region of the spray, if the velocity at any radial position is divided by the centreline velocity and plotted versus the normalized radius ( $r/R$ ), where  $r$  is the radial coordinate and  $R$  the spray radius defined from the velocity angle  $\theta_u$  (see figure 1), it has a single evolution.

This result can be expressed as:

$$U(x,r) = U(x,0)f(r/R) \quad (1)$$

where  $f$  is a radial profile for the variable  $U$ . The same result is obtained if fuel concentration is considered:

$$C(x,r) = C(x,0)[f(r/R)]^{Sc} \quad (2)$$

where  $Sc$  is the effective Schmidt number.

The Schmidt number is the ratio of effective momentum diffusivity to effective mass diffusivity and represents the relative rate of momentum and mass transfer, including both molecular and turbulent contributions. It is defined as:

$$Sc = \frac{\nu}{D} \quad (3)$$

with  $\nu$  the kinematic viscosity, and  $D$  the mass diffusivity.

An immediate consequence of self-similarity is that a significant simplification can be made when presenting results: only centreline axial velocity and fuel concentration are required, as values for any other point can be deduced from centreline values.

## 2.2. Theoretical derivation

In order to rigorously impose momentum flux conservation in a free gas jet or a diesel spray, it is necessary to take into account the radial evolution of both axial velocity and fuel concentration. For any section perpendicular to the spray axis in the steady region of the gas jet or diesel spray, momentum flux is conservative, and thus equal to that existing at the nozzle exit (Payri, R. *et al.* 2005).

Consequently, the following equation can be written:

$$\dot{M}_o = \dot{M}(x) \quad (4)$$

where  $\dot{M}_o$  and  $\dot{M}(x)$  are the momentum flux through a spray cross section at the orifice outlet and at a distance  $x$ , respectively. It can be assumed that the radial profile of the velocity at the nozzle exit is flat, and thus  $\dot{M}_o = \dot{m}_f U_o$ , where  $\dot{m}_f$  is the mass flux, and  $U_o$  the orifice outlet velocity. Influences of a non-flat profile have been studied by Post *et al.* (2000). They show that, if the mass and axial momentum fluxes are the same, the influence of the profile shape is confined to the initial region. In the main jet region, the distribution of axial velocity is identical at any axial position.

In order to develop expression (4), momentum must be integrated over the whole section, assuming cylindrical symmetry of the spray or jet:

$$\dot{M}_o = \dot{M}(x) = \int_0^{\infty} 2\pi\rho(x,r)rU^2(x,r)dr \quad (5)$$

where the  $x$ -coordinate coincides with the spray axis, and the  $r$ -coordinate is the radial position (perpendicular to the spray axis). In this expression,  $U(x,r)$  is the local spray velocity and  $\rho(x,r)$  is the local density in the gas jet or diesel spray defined as:

$$\rho(x,r) = \frac{m_a + m_f}{V_a + V_f} \quad (6)$$

being  $m_f$  and  $V_f$  the local mass and volume of fuel, and  $m_a$  and  $V_a$  the local mass and volume of air.

The density at an internal point of the spray, taking into account the local concentration, can be written in terms of spray local concentration as follows (complete derivation can be seen in Appendix A):

$$\rho(x,r) = \rho_f \frac{1}{C(x,r) \left(1 - \frac{\rho_f}{\rho_a}\right) + \frac{\rho_f}{\rho_a}} \quad (7)$$

with  $\rho_f$  the fuel density,  $\rho_a$  the air density and  $C(x,r)$  the local (mass-based) fuel concentration, defined as:

$$C(x,r) = \frac{m_f}{m_a + m_f} \quad (8)$$

whose value can be significantly different from the local volume concentration, which is also frequently used in sprays studies (more details can be seen in the Appendix A).

For the developed region in the spray, fuel concentration and axial velocity can be considered to follow a Gaussian radial profile:

$$U(x,r) = U_{axis}(x) \exp\left(-\alpha \left(\frac{r}{R}\right)^2\right) \quad (9)$$

$$C(x,r) = C_{axis}(x) \exp\left(-\alpha Sc \left(\frac{r}{R}\right)^2\right) \quad (10)$$

with  $Sc$  the Schmidt number, and  $\alpha$  the shape factor of the Gaussian distribution. At this point it is necessary to point out that radial distributions of axial velocity are not well known in sprays. Some authors use gas jet distributions as a first approximation. Experimental similarities between them have been always remarked by other researchers (Adler and Lyn 1969; Prasad and Kar 1976; Sinnamon *et al.* 1980; Correas 1998; Desantes *et al.* 2006a). Different expressions for radial profiles can be found in the literature (Abramovich 1963; Hinze 1975; Schlichting 1978; Spalding 1979; Sinnamon *et al.* 1980). Correas (1998) made a

comparative study of all of them, and proposed a modification of the expressions by Hinze (1975), which has often been considered as the profile that best fits the available experimental data in the literature. This profile was also assumed by the authors of this paper in more recent studies (Desantes *et al.* 2006a, Desantes *et al.* 2007; Payri, R. *et al.* 2008). Even though it is included here as an assumption, results obtained with a PDPA (Phase Doppler Particle Analyzer) system will be presented in the next sub-section as a summary of those presented in Desantes *et al.* (2007); Payri, R. *et al.* (2008), which will show that the Gaussian profile is a proper approach for the type of sprays within the scope of the present work. Additionally, Yue *et al.* (2001) have verified that the Gaussian distributions can reproduce results obtained via x-ray radiography rather accurately. Substituting Eqs. (7), (9) and (10) in Eq. (5), the momentum in any section of the spray can be expressed as:

$$\dot{M}_o = 2\pi\rho_f U_{axis}^2 \times \int_0^{\infty} \frac{r \cdot \exp\left(-2\alpha\left(\frac{r}{R}\right)^2\right)}{C_{axis} \left(1 - \frac{\rho_f}{\rho_a}\right) \exp\left(-\alpha Sc \left(\frac{r}{R}\right)^2\right) + \frac{\rho_f}{\rho_a}} dr \quad (11)$$

Integrating Eq. (11) and taking into account that the radius of the spray  $R$  can be expressed with respect to the spray velocity angle as:

$$R = x \tan\left(\frac{\theta_u}{2}\right) \quad (12)$$

the following expression is obtained (details of the steps followed in integration can be found in Desantes *et al.* 2007):

$$\dot{M}_o = \frac{\pi}{2\alpha} \rho_a \tan^2\left(\frac{\theta_u}{2}\right) x^2 U_{axis}^2 \sum_{i=0}^{\infty} \frac{1}{\left(1 + i \frac{Sc}{2}\right)} \left[ C_{axis} \left( \frac{\rho_f - \rho_a}{\rho_f} \right) \right]^i \quad (13)$$

In this expression, spray velocity angle  $\theta_u$  is defined as the angle at which velocity reaches 1% of its value at spray axis which is assumed to be constant along the spray axis, and  $i$  is the index for the summation which approximates the solution of the integration seen in Equation (11). The previous equation is very interesting because it relates momentum flux with velocity on the axis for a given position, density in the chamber, spray cone angle and  $Sc$  number. For this model, the following assumptions are explicitly made:

- Cylindrical symmetry and Gaussian profiles are assumed for spray microscopic characteristics.
- The environment is quiescent and so no axis deflection exists.
- Air density in the injection chamber is constant during the whole injection process.
- Momentum and thus injection velocity and mass flow rate are constant during the whole injection process.
- Slip between gas and liquid phases is negligible.

The authors found in Desantes *et al.* (2007) that, for a given set of conditions, Schmidt number variations between 0.6 and 1.4 did not have any significant influence on the calculated on-axis velocities for the spray region beyond approximately  $20\phi_{eq}$  (with  $\phi_{eq} = \phi_o \sqrt{\rho_f / \rho_a}$ ),  $\phi_{eq}$  being the equivalent diameter and  $\phi_o$  the outlet diameter of the nozzle. Nevertheless, the influence of Schmidt number becomes very important in the near-nozzle field as it will be seen in section 4 where some measurements of mass distribution are performed. The consequence is that when  $Sc$  is not known, which is normally the case, a simplified equation for  $Sc=1$  can be expected to give very good estimations far from the nozzle exit, as it will be demonstrated in next section. This hypothesis implies that the diffusion rates of these two parameters are the same, and so, mass concentration and velocity profiles have the same radial profile (according to eqs. 1 and 2).

Another possible simplification refers to the consideration of a constant density in the chamber (and thus, inside the spray) equal to the air density in the chamber in the injection chamber. This assumption can only be made far from the nozzle exit, where droplets are dispersed, so that the mass and volume occupied by fuel can be considered negligible with respect to the entrained air. According to Desantes *et al.* (2007), assuming that the density is constant inside the spray and equal to the ambient one, Equation (13) can be further simplified. In fact, if  $\rho(x,r) = \rho_a$ , the integration of Equation (5) simplifies and leads to Equation (14):

$$U_{axis} = \frac{\dot{M}_o^{1/2}}{\rho_a \left( \frac{\pi}{2\alpha} \right) x \tan \left( \frac{\theta_u}{2} \right)} \quad (14)$$

The authors (Desantes *et al.* 2007) compared the velocity in the axis calculated from Equation (14) (constant density) with that obtained from Equation (13) (local density variations with  $Sc=1$ ) and they found that the main differences occur very close to the orifice because in this initial part of the spray, the local density is far from constant. Nevertheless, beyond  $30\phi_{eq}$  the differences are less than 3%. This is due to the fact that the constant density assumption starts becoming valid as the jet develops and spreads apart.

### 2.3. Experimental support and validation using momentum flux measurements and PDPA measurements

The spray momentum can be measured experimentally with good reliability and precision by simply employing a sensor that measures the impact force of the spray on a plate perpendicular to its axis (Payri, R. *et al.* 2005)

From the theoretical point of view and considering Equation (13), apart from the spray momentum, the half spray cone angle is also needed for the model predictions. This parameter can be obtained from a fitting of the exponential function to the normalized profiles of axial velocity. Velocity fields measured with the PDPA system can be used for that purpose.

As an example, in Figure 2a, the velocity values normalized by the spray axis velocity are plotted in terms of normalized coordinates ( $r/x$ ) for a tapered nozzle with 126 micrometers of nozzle diameter and for two different injection pressures: 30 MPa and 80 MPa. The density in the chamber was  $40 \text{ kg/m}^3$  at room temperature. The accuracy of the PDPA technique at these conditions has been estimated as  $\pm 5\%$ . From these experimental points, a fit has been performed to the function  $\exp(k(r/x)^2)$  which is also plotted as a dotted line in Figure 2a. The constant  $k$  coming from the previous fitting of the velocity measurements can be compared to the expression of the Gaussian profile seen in Equation (9). Thus, spray velocity angle can be obtained from the following expression:

$$k = \frac{-\alpha}{\tan^2\left(\frac{\theta_u}{2}\right)} \quad (15)$$

with  $\alpha$  the shape factor of the Gaussian distribution equal to 4.6 according to Desantes *et al.* (2007) and Payri, R. *et al.* (2008). The figure clearly demonstrates the suitability of the Gaussian profiles for the velocity fields. The same conclusion was obtained in Payri, R. *et al.* (2008) involving three different nozzles and injection conditions. Furthermore, a comparison of different radial profiles available in the literature is made in Appendix B, showing that Gaussian profiles proposed in Equation (9) give the most accurate estimation for spray velocity radial distribution.

On the other hand, in Figure 2b the results of spray droplet velocity measured in the spray axis at different axial positions for the same nozzle, but in this case at three different injection pressures (30 MPa, 80 MPa and 130 MPa) and two different ambient densities (25 kg/m<sup>3</sup> and 40 kg/m<sup>3</sup>), are presented. As stated before, at this distance, variations due to Schmidt number or local density variations are already negligible, and so, the simplified Equation (14) is enough in order to compare theoretical results with those obtained experimentally. In this case, and taking into account Equation (14), the information needed is the spray momentum flux and the velocity cone angle previously determined. As far as the momentum flux is concerned, the values obtained for this nozzle at 30 MPa, 80 MPa and 130 MPa of injection pressure were 0.62 N, 1.61 N and 3.05 N for full needle lift conditions. As it can be seen from the figure, the agreement between the model and the experimental data is fairly good. As for the radial profiles, further conditions and nozzles are evaluated in Payri, R. *et al.* (2008).

### **3. Analysis of x-ray mass distribution measurements**

Up to this point, the experimental data available have allowed a validation in the main region of the spray but not quite in the initial region (see Figure 1). From now on, a fruitful combination of the model and x-ray measurements near the initial region of the spray will allow extracting information about mass and momentum transfer in the nozzle vicinity.

### 3.1. Measurement basis

Quantification of spray characteristics such as fuel concentration, velocity or droplet size has been the aim of numerous studies. In order to carry out non-intrusive measurements, several optical techniques have been used for this purpose. Nevertheless, most of these techniques are limited to the edge of the spray, where fuel concentrations are low.

On the contrary, the x-ray absorption technique developed by Argonne National Laboratories has recently shown to be helpful to understand spray behaviour in the dense core of the spray (Leick *et al.* 2007; Tanner *et al.* 2006; Ramirez *et al.* 2009). Visible light is highly scattered by fuel parcels, so the intensity is rapidly attenuated. Instead of this, x-ray beams are mainly absorbed by fuel, but the intensity remaining after the passage through the dense core region remains high enough to be accurately measured. The intensity loss of monochromatic x-ray beams inside the spray is related with the fuel mass present in the beam path:

$$\frac{I}{I_0} = \exp(-\mu_m M') \quad (16)$$

$I$  being the x-ray beam intensity measured after the spray by a photodiode,  $I_0$  the incident x-ray intensity, and  $\mu_m$  the absorption constant.  $M'$  is the projected fuel mass per unit area along the x-ray beam path, which can be defined as:

$$M' = \int \rho_L(z) dz \quad (17)$$

where  $\rho_L$  is the local fuel density, defined as  $\rho_L = \frac{m_f}{V_a + V_f}$ , and  $z$  is the axis that

defines x-ray beam direction, perpendicular to the spray. The definition of local fuel density differs from the local spray density seen before ( $\rho$ ), as it only contemplates the fuel mass, due to the fact that x-ray absorption by the air entrained into the jet is negligible. A scheme of the experimental setup is shown in Figure 3a.

Equation (17) gives the relationship between the experimental parameter  $M'$  and local spray characteristics in terms of density. It can be demonstrated that local fuel density can be expressed as a function of local concentration (more details can be seen in Appendix A):



$$\rho_L(x, r) = \frac{\rho_f}{\left(1 - \frac{\rho_f}{\rho_a}\right) + \frac{1}{C(x, r)} \frac{\rho_f}{\rho_a}} \quad (18)$$

As it was stated in Equation (10),  $C(x, r)$  can be expressed as

$$C(x, r) = C_{axis}(x) \exp\left(-\alpha S_c \left(\frac{r}{R}\right)^2\right) \quad (19)$$

In this expression,  $R$  is the spray radius at axial position  $x$ , defined as  $R = x \tan(\theta_u/2)$ . This radius can be calculated in terms of mass angle instead of velocity angle (see Figure 1) using the following relationship:

$$\tan\left(\frac{\theta_u}{2}\right) = \sqrt{S_c} \tan\left(\frac{\theta_m}{2}\right) \quad (20)$$

So that local concentration can be calculated as:

$$C(x, r) = C_{axis}(x) \exp\left(-\alpha \left(\frac{r}{x \tan(\theta_m/2)}\right)^2\right) \quad (21)$$

Introducing this expression of  $C(x, r)$  into Equation (18), and defining

$R_m = x \tan(\theta_m/2)$ , local fuel density can be expressed as:

$$\rho_L(x, r) = \frac{\rho_f}{\left(1 - \frac{\rho_f}{\rho_a}\right) + \frac{1}{C_{axis}(x) \exp\left(-\alpha \left(\frac{r}{R_m}\right)^2\right)} \frac{\rho_f}{\rho_a}} \quad (22)$$

where spray mass angle  $\theta_m$  is defined as the angle at which concentration reaches 1% of its value at spray axis at any axial position.

In order to be related with experimental  $M'$  values, and so to extract as much information as possible, local fuel density must be expressed in terms of the position in path direction  $z$  instead of in terms of radial position  $r$ . For this purpose, and as depicted in Figure 3b, the following change of variable is needed:

$$r = \left(r_i^2 + z^2\right)^{1/2} \quad (23)$$

where  $r_i$  is the radial position of the x-ray beam at the  $z = 0$  plane.

Taking into account Equations (22) and (23), Equation (17) can be transformed into:

$$M' = \int_{-\infty}^{+\infty} \frac{\rho_f}{\left(1 - \frac{\rho_f}{\rho_a}\right) + \frac{1}{C_{axis}(x) \exp\left(-\alpha \left(\frac{r_i^2 + z^2}{R_m^2}\right)\right)} \frac{\rho_f}{\rho_a}} dz \quad (24)$$

This equation is very useful because it enables to relate the variable  $M'$ , determined experimentally by the x-ray technique, to other more important parameters such as local fuel concentration or spray radius (and, consequently, spray cone angle). Additionally, this reasoning can be followed to analyze x-ray results at any axial position or experimental setup, with the only assumption that spray characteristics can be described using Gaussian profiles, as stated in Equation (19).

### 3.2. Analysis of radial profiles

In previous studies developed at Argonne National Laboratories (Leick *et al.* 2007; Tanner *et al.* 2006; Ramirez *et al.* 2009), information about  $M'$  values was obtained for two different nozzles at several radial positions  $r_l$ . These results concerned two different experimental setups (including different nozzles, injection and discharge pressure conditions and also different axial positions for the x-ray beam), giving a total amount of 25 measurements.

The first set of measurements chosen for the current analysis (Test 1) is reported in Leick *et al.*'s study (2007). In this paper, a 3-hole tapered VCO nozzle with an outlet diameter of 0.145 mm and a  $k$ -factor of 1.5 is mounted on a Bosch common rail injector. X-ray measurements are performed in a constant volume vessel; injection pressure is 80 MPa and the chamber is filled with nitrogen at a density of 21.7 kg/m<sup>3</sup>. The same methodology has been used in Tanner *et al.* (2006), using a single-hole nozzle with a diameter of 0.180 mm, an injection pressure of 50 MPa and a chamber pressure of 0.5 MPa, leading to a chamber density of 5.65 kg/m<sup>3</sup> (Test 2). A diesel fuel/cerium blend ( $\rho_f = 890$  kg/m<sup>3</sup>) has been used for the two tests. All the experimental tests were carried out at room temperature. A summary of these two experimental setups, as well as the experimental data available, are shown in Figure 4.

These experimental results can be analyzed with the aid of Equation (24) in order to extract physical information about fuel concentration inside a diesel spray, as well as to validate Gaussian radial profiles proposed in Equations (9) and (10) in

the near-nozzle field. Nevertheless, Equation (24) does not have an analytical solution and, moreover, it involves two unknown parameters: axial concentration and mass angle (involved in  $R_m$  definition). For this reason, a numerical procedure has been defined in order to determine these parameters. A scheme of this procedure is shown in Figure 5.

As it can be seen, a wide range of  $\theta_m$  is tested (from 5 to 30°, with an angle step of 0.25°). For each of these values, also a range for  $C_{axis}$  is used (from 0.5 to 1, with a concentration step of 0.001), giving a total number of 50601 combinations of these two parameters. Each combination of  $\theta_m$  and  $C_{axis}$ , together with the experimental conditions described in Figure 4, allows the calculation of  $M'$  at each one of the  $n_r$  radial measuring positions, giving a radial distribution of  $M'$ . This distribution can be compared with the experimental data using the following expression:

$$\mathcal{E}_{\theta_m C_{axis}} = \frac{\sqrt{\sum_{r_1=0}^{R} [M'_{\theta_m C_{axis}}(r_1) - M'_{ex}(r_1)]^2}}{n_r} \quad (25)$$

where  $\mathcal{E}_{\theta_m C_{axis}}$  is the mean deviation obtained between the predicted and experimental values of the whole radial  $M'$  distribution at a fixed  $\theta_m$  and  $C_{axis}$  combination,  $M'_{\theta_m C_{axis}}(r_1)$  and  $M'_{ex}(r_1)$  are the predicted and the experimental values at each radial position and  $n_r$  is the total amount of radial positions measured.

A minimization of the deviation parameter defined in Equation (25) can be developed in order to obtain the  $\theta_m$  and  $C_{axis}$  combination that best fits with the experimental results. A 3-D surface plot of the average deviation in terms of the two parameters considered for the predictions ( $\theta_m$  and  $C_{axis}$ ) for Test 1 conditions is shown in Figure 6. As it can be seen, average deviation function has a global minimum at  $\theta_m = 20.25$  degrees and  $C_{axis} = 0.933$ . Thus, it can be established that this combination produces the optimal estimation of the experimental results for these conditions, with a maximum uncertainty equal to the step value considered for each parameter (0.25 for spray angle and 0.001 for axial concentration). Similar behaviour is obtained for Test 2 conditions, arriving to values of  $\theta_m = 14$  degrees and  $C_{axis} = 0.954$ . The results of the optimization are summarized in Table 1 for the test conditions already described.

As it can be seen, the mean deviation obtained for these two predictions is low enough to assure that these parameters reproduce properly the experimental results (lower than 5% of the centre line value). To corroborate the quality of this approach, comparison of experimental and predicted radial  $M'$  profiles are represented in Figure 7. It can be seen that the estimated values reproduce experimental data with a high degree of confidence. This way, Gaussian profiles introduced in section 2 are shown to be adequate to reproduce spray characteristics even in the near-nozzle field.

### 3.3. Evolution along the spray axis

As it has been shown in section 2.2, the Schmidt number determines not only the radial distribution of local concentration and velocity, but also the evolution of these parameters along the spray axis. Thus,  $M'$  axial evolution could be used to characterize the  $Sc$  in diesel sprays. This kind of information was also available for the same nozzle and conditions of Test 1 radial analysis already described (Leick *et al.* 2007).

With the aim of evaluating the Schmidt number in these conditions, the first step has consisted in calculating the concentration  $C_{axis}(x)$  at every axial position at which  $M'$  has been measured.

As it was seen in the previous radial analysis, Equation (24) relates  $M'$  and axial concentration ( $C_{axis}$ ) at a given position  $x$ . Introducing the value of spray mass angle calculated in the previous section, Equation (24) can be used to obtain directly the evolution of  $C_{axis}$ . Again, this equation does not have an analytical solution, so a numerical procedure must be followed.  $C_{axis}$  between 0.5 and 1 has been tested at each axial position, giving a numerical value  $M'_{C_{axis}}$ , and so deviation between experimental and predicted values can be calculated as:

$$\varepsilon_{C_{axis}}(x) = \frac{\sqrt{[M'_{C_{axis}}(x) - M'_{ex}(x)]^2}}{M'_{ex}(x)} \quad (26)$$

which has been minimized. Optimal  $M'$  values obtained following this procedure are plotted together with experimental values in Figure 8.a. Additionally, the values of axial concentration obtained from the optimization process performed at each axial position are represented in Figure 8.b. As it can be seen, experimental and predicted  $M'$  values are almost equal except in the initial region of the spray.

This result can be due to the fact that some hypotheses used in the theoretical derivation (as the Gaussian profiles) cannot be applicable in the initial region of the spray, where axial concentration is equal to the unity.

In order to gain knowledge about the influence of  $Sc$  on the axial evolution of spray concentration, the values of  $C_{axis}$  which minimized the error in the  $M'$  prediction can be compared to the behaviour predicted by the theoretical model already described in section 2.

In this model, as seen in Equation (13), axial spray behaviour is described in terms of momentum flux, outlet velocity and axial concentration. Momentum flux at the nozzle exit can also be calculated as:

$$\dot{M}_o = \rho_f A U_o^2 \quad (27)$$

where  $A$  is the section of the outlet hole of the nozzle. So that Equation (13) can then be easily transformed into:

$$\rho_f A = \frac{\pi}{2\alpha} \rho_a \tan^2\left(\frac{\theta_u}{2}\right) x^2 \left(\frac{U_{axis}}{U_o}\right)^2 \sum_{i=0}^N \frac{1}{\left(1+i\frac{Sc}{2}\right)} \left[ C_{axis} \left(\frac{\rho_f - \rho_a}{\rho_f}\right) \right]^i \quad (28)$$

where  $N$  is the number of terms for the truncation of the series defined in Equation (13), necessary for the numerical calculation of the series value. Previous analyses have shown that axial concentration and velocity can be related with the aid of the Schmidt number (Desantes *et al.* 2006b). In particular, the following expression has shown to perform properly in the near-nozzle field:

$$\left(\frac{U_{axis}}{U_o}\right) = C_{axis}^{Sc} \quad (29)$$

If this definition is introduced in Equation (13), an implicit equation for the  $Sc$  in terms of  $C_{axis}$  can be stated:

$$1 = \frac{\pi}{2\alpha} \frac{\rho_a}{\rho_f} \frac{1}{A} \tan^2\left(\frac{\theta_u}{2}\right) x^2 (C_{axis})^{2Sc} \sum_{i=0}^N \frac{1}{\left(1+i\frac{Sc}{2}\right)} \left[ C_{axis} \frac{\rho_f - \rho_a}{\rho_f} \right]^i \quad (30)$$

Finally, Equation (20) can be used to express Equation (30) in terms of mass angle:

$$1 = \frac{\pi}{2\alpha} \frac{\rho_a}{\rho_f} \frac{1}{A} Sc \tan^2\left(\frac{\theta_m}{2}\right) x^2 (C_{axis})^{2Sc} \sum_{i=0}^N \frac{1}{\left(1 + i \frac{Sc}{2}\right)} \left[ C_{axis} \frac{\rho_f - \rho_a}{\rho_f} \right]^i \quad (31)$$

where  $\theta_m$  is the spray mass angle at an axial position of 4 mm (section 3.2, test 1 conditions). This value is assumed to be constant for any axial position.

This expression cannot be solved analytically, but numerical methods can be applied in order to have a solution in terms of  $C_{axis}$  for the different axial positions. Although previous analysis have pointed out that the solution given by this model is independent of  $N$  for values higher than 7-9 (Desantes *et al.* 2006a), the current calculation has been developed for  $N = 11$ , in order to assure a high degree of accuracy. In particular, the truncation error of the series would represent around 1.5-2% for typical values of  $Sc$  and  $C_{axis}$ , so that it can be concluded that the resolution with 11 terms is adequate. Using this expression, a comparison of experimental and theoretical axial evolution of  $C_{axis}$  can be obtained and shown in Figure 9. In this figure, theoretical axial profiles of  $C_{axis}$  are evaluated at different Schmidt numbers using Equation (31), together with  $C_{axis}$  values obtained from experimental  $M'$  data.

As it can be seen, there are three different zones attending to the behaviour of  $C_{axis}$  in terms of  $Sc$ . The first zone corresponds to the initial region of the spray, where axial concentration is equal to one. The length of this zone is better reproduced as the  $Sc$  chosen for calculation gets higher. The final zone (beyond ~3.5 mm) shows a good agreement with the results given by the theoretical model for a  $Sc$  value near 0.5. This value is lower than those observed by Prasad and Kar (1976), but it must be considered that their study was developed under quite different conditions ( $P_{in} < 20$  MPa,  $\phi_o > 0.4$  mm,  $P_{back} = 0.1$  MPa). Furthermore, they found that  $Sc$  decreased as injection pressure got higher, which would imply that values lower than 0.7 could be expected under modern engine conditions, as it has been obtained in the current study.

In the transitional region (from 2 to 3.5 mm), the behaviour of  $C_{axis}(x)$  does not correspond with any theoretical curve. This could be due to different reasons:

- The Schmidt number could not be constant along the spray axis. In fact, as it has been explained, high  $Sc$  values would reproduce more properly spray parameters as the length at which  $C_{axis} = 1$ . An evolution of  $Sc$  from values

near unity to the fully developed value of 0.5 could explain the experimental evolution of  $C_{axis}$ .

- Spray cone angle has been supposed to be constant along the whole spray. Nevertheless, recent investigation works based on visualization techniques have pointed out that spray angle near the nozzle exit is significantly different from the expected cone angle defined at higher axial positions (Linne *et al.* 2006, Saliba *et al.* 2004, Heimgärtner and Leipertz 2000).
- The proposed model uses the gaseous jet analogy. For this reason, this model can only be useful to characterize spray behaviour at positions at which atomization has already taken place and fuel has been decomposed in droplets small enough to behave in a similar way to a gas jet.

### 3.4. Application of previous results

The previous analyses based on x-ray measurements have allowed the determination of spray cone angle for two different nozzles and pressure conditions, as well as an estimation of the Schmidt number from axial measurements for one of them. The importance of these parameters is based on the possibility of predicting spray behaviour by means of the theoretical model described in section 2 once these parameters are known. In this sense, Figure 10 shows local velocity and concentration contours for the two experimental setups analyzed in this paper. For this purpose, although the Schmidt number estimation has been developed only for Test 1 conditions, the same value has been assumed for the Test 2, where only the value of the spray mass angle has been adapted. These contours summarize the air-fuel mixing process in the first 15 millimetres of the spray. It can be seen that the mixing process is more effective for Test 1 conditions, mainly due to the higher chamber density, which is known to have a decisive influence. Thus, it is appreciable that spray concentration drops faster along the axial direction for Test 1 conditions, and that spray widening is more pronounced. The black zone in these contour maps can be immediately related with the length of the initial region of the spray. This length, defined as the position at which axial concentration reaches unity, is an important parameter in order to analyze air-fuel mixing process. Again, it is seen that higher density induces a shorter length of the  $C_{axis} = 1$  region ( $\sim 3.2$  mm) with respect to Test 2 conditions ( $\sim 9$  mm). Remembering Figure 9, the simplified model overestimated

the length of the region at which  $C_{axis} = 1$ , due to the inaccuracies of the model in this region. For this reason, shorter lengths should be expected in reality.

Another noticeable aspect is the strong difference between local velocity and concentration contours. Paying attention to the edge of the spray in these contour maps (defined as 1% of the maximum concentration or velocity), it can be seen that the concentration contour is much wider than the velocity one. This is due to the fact that the Schmidt number, defined as the ratio between viscosity and mass diffusivity, is considerably smaller than 1, which indicates that momentum transfer is less effective than mass transfer. In particular, Equation (19) indicates that  $\tan(\theta_w/2) = 0.75 \tan(\theta_m/2)$  for a  $Sc$  of 0.5. This relationship explains the differences seen between velocity and concentration contours.

## 4. Conclusions

A theoretical analysis combined with experimental measurements of momentum flux, droplet velocity (using a Phase Doppler Particle Analyzer) and mass distribution with x-ray radiography has been used in this research, which has made it possible to better understand the behaviour of diesel spray dynamics. The theoretical development is based on physical considerations and on empirical evidence.

From this work, the following conclusions can be drawn:

- As a result of a theoretical reasoning based on momentum flux conservation in the axis direction of the diesel spray, a mathematical model has been obtained which relates the momentum flux with the profiles of velocity and concentration, local density and spray cone angle.
- Some experimental results of droplet velocity measured with the PDPA technique have been used to validate the model obtaining acceptable agreement between experimental measurements and the theoretical model.
- X-ray projected mass distribution measurements have shown to be useful in order to characterize spray behaviour in the near-nozzle field, where the influence of Schmidt number is more severe. Information from two different nozzles, experimental setups and axial positions were available.
- The analysis of the x-ray measurements has led to the conclusion that the Gaussian profiles proposed reproduce properly experimental data available from the near-nozzle region.



- When analyzing axial distribution of  $M'$ , the best fit for experimental measurements is obtained for a Schmidt number around 0.5 for axial positions higher than 3.5 mm. Nevertheless, for  $x < 3.5$  mm, there is no value of  $Sc$  that reproduces the axial distribution of  $C_{axis}$ . Furthermore, it can be seen that the initial region length (position at which  $C_{axis}$  is 1) is better reproduced as  $Sc$  is increased. This could indicate that the Schmidt number is varying in the first millimeters of the spray until it arrives at its full-developed value. Also variation of spray angle during this transitional region could explain this phenomenon.
- Once the Schmidt number and the spray cone angle are known for a set of experimental conditions, the theoretical approach already described allows the complete characterization of spray behaviour in terms of velocity and local concentration. In this sense, contour plots of these parameters for the two nozzles analyzed in this paper have been developed and analyzed.

## Appendix A

Local density  $\rho$  can be defined as the ratio between the total mass and volume at a given location of the spray:

$$\rho(x,r) = \frac{m_a + m_f}{V_a + V_f} \quad (32)$$

being  $m_f$  and  $V_f$  the local mass and volume of fuel, and  $m_a$  and  $V_a$  the local mass and volume of air.

Together with this local density, local volume and mass concentrations can be defined as:

$$C_v(x,r) = \frac{V_f}{V_a + V_f}; \quad C(x,r) = \frac{m_f}{m_a + m_f} \quad (33)$$

Using these definitions, local density can be rewritten as:

$$\rho(x,r) = \frac{m_a + m_f}{V_a + V_f} = \frac{m_f / C}{V_f / C_v} = \rho_f \frac{C_v(x,r)}{C(x,r)} \quad (34)$$

Dividing local mass and volume concentrations:

$$\begin{aligned}\frac{C(x,r)}{C_v(x,r)} &= \frac{m_f}{m_a+m_f} \frac{V_a+V_f}{V_f} = \frac{m_f}{m_a+m_f} \cdot \frac{m_a/\rho_a+m_f/\rho_f}{m_f/\rho_f} = \\ &= \rho_f \left[ \frac{1}{\rho_a} \frac{m_a}{m_a+m_f} + \frac{1}{\rho_f} \frac{m_f}{m_a+m_f} \right] = \frac{\rho_f}{\rho_a} (1-C(x,r)) + C(x,r)\end{aligned}\quad (35)$$

Introducing this expression into the local density definition, it can be seen that:

$$\rho(x,r) = \rho_f \frac{C_v(x,r)}{C(x,r)} = \frac{\rho_f}{\frac{\rho_f}{\rho_a} (1-C(x,r)) + C(x,r)} = \frac{\rho_f}{\frac{\rho_f}{\rho_a} + C(x,r) \left(1 - \frac{\rho_f}{\rho_a}\right)} \quad (36)$$

Additionally, local fuel density can be defined as:

$$\rho_L(x,r) = \frac{m_f}{V_a+V_f} \quad (37)$$

This definition is useful for the analysis of x-ray measurements, as the absorption by the air mass is almost negligible. It can be seen that there is a direct relationship between local fuel density  $\rho_L$  and local density  $\rho$ :

$$\rho(x,r) \cdot C(x,r) = \frac{m_a+m_f}{V_a+V_f} \cdot \frac{m_f}{m_a+m_f} = \frac{m_f}{V_a+V_f} = \rho_L(x,r) \quad (38)$$

So that local fuel density can be expressed in terms of local concentration as:

$$\rho_L(x,r) = \frac{\rho_f C(x,r)}{\frac{\rho_f}{\rho_a} + C(x,r) \left(1 - \frac{\rho_f}{\rho_a}\right)} = \frac{\rho_f}{\frac{1}{C(x,r)} \frac{\rho_f}{\rho_a} + \left(1 - \frac{\rho_f}{\rho_a}\right)} \quad (39)$$

## Appendix B

A summary of some of the most relevant radial profiles available in the literature for the characterization of spray velocity is made in Table 2. In these expressions, spray width must be adjusted by experimental results. For this purpose, two parameters can be defined:

- Spray radius ( $R$ ), which can be calculated in terms of spray velocity angle as:

$$R = x \tan\left(\frac{\theta_u}{2}\right) \quad (40)$$

- $r_{1/2}$ , which is defined as the radial position at which spray velocity reaches 50% of its maximum value.

These profiles can be used to approach experimental data of spray velocity obtained from a Phase Doppler Particle Analyzer (PDPA), presented in section 2.3. The reproduction of the experimental data by each of these expressions is seen in Figure 11.a.

As it can be seen, experimental data is properly reproduced for all the expressions, with the only exception of the one proposed by Spalding (1979). Nevertheless, in order to quantify the capability of each one of these radial profiles to reproduce the experimental data, mean squared deviation between predictions and experiments (*MSD*) is calculated as:

$$MSD = \frac{\sqrt{\sum_{j=1}^{n_{ex}} [U_{mo}(x_j, r_j) - U_{ex}(x_j, r_j)]^2}}{n_{ex}} \quad (41)$$

$U_{ex}(x_j, r_j)$  being the velocity values obtained in the PDPA measurements at the experiment  $j$ ,  $U_{mo}(x_j, r_j)$  the predicted value given by each model at the same operating conditions,  $x_j$  and  $r_j$  the measuring position for experiment  $j$ , and  $n_{ex}$  the total number of measurements available from PDPA system.

As it can be seen in Figure 11.b, Gaussian fit proposed by the authors shows the lowest MSD values for both injection pressure values considered in the analysis. Radial profile proposed by Schlichting (1978) gives results with similar accuracy, while the other two profiles are considerably less accurate in their prediction. Considering these results, Gaussian profiles described in Equations (8) and (9) would be the best option for the spray analysis performed afterwards in terms of MSD. Nevertheless, the differences between the radial profiles tested are slight, so that any of them would be acceptable to reproduce the experimental results.

## Acknowledgement

This work was partly sponsored by “Vicerrectorado de Investigación, Desarrollo e Innovación” of the “Universidad Politécnica de Valencia” in the frame of the project “Estudio del flujo en el interior de toberas de inyección Diesel”, reference N° 3150 and by “Generalitat Valenciana” in the frame of the project with the same title and reference GV/2009/031.

This support is gratefully acknowledged by the authors.

## References

- Abramovich GN (1963) The theory of turbulent jets. MIT Press.
- Adler D, Lyn WT (1969) The evaporation and mixing of a liquid fuel spray in a Diesel air swirl. Proc. Instn. Mech. Engrs. 184: 171-180.
- Coghe A, Cossali GE (1994) Phase Doppler characterisation of a Diesel spray injected into a high density gas under vaporisation regimes. 7th Int. Symp. On Appl. Of Laser Tech. To Fluid Mech., Lisbon.
- Correas D (1998) Theoretical and experimental study of isothermal Diesel free sprays (In Spanish). PhD Thesis, Universidad Politécnica de Valencia.
- Cossali GE (2001) An integral model for gas entrainment into full cone sprays. J. Fluid Mech. 439: 353-366.
- Dent JC (1971) A basis for the comparison of various experimental methods for studying spray penetration. SAE Paper 710571.
- Desantes JM, Payri R, Salvador FJ, Gil A (2006a) Deduction and validation of a theoretical model for a free Diesel Spray. Fuel 85: 910-917.
- Desantes JM, Arrègle J, López JJ, Cronhjort A (2006b) Scaling laws for free turbulent gas jets and Diesel-like sprays. Atomization Spray 16: 443-473.
- Desantes JM, Payri R, García JM, Salvador FJ (2007) A contribution to the understanding of isothermal diesel spray dynamics. Fuel 86: 1093-1101.
- Dumouchel C (2008) On the experimental investigation on primary atomization of liquid streams. Exp. Fluids 45: 371:422.
- Heimgärtner C, Leipertz A (2000) of the primary spray break-up close to the nozzle of a common-rail high pressure Diesel injection system. SAE Paper 2000-01-1799.
- Hinze JO (1975) Turbulence. McGraw-Hill.
- Hiroyasu H, Arai M (1990) Structures of fuel sprays in Diesel engines. SAE Paper 900475.
- Jawad B, Gulari E, Henein NA (1992) Characteristics of intermittent fuel sprays. Combust. flame 88: 384-396.
- Lefèbvre AH (1989) Atomization and Sprays. Hemisphere Publishing Corporation.
- Leick P, Riedel T, Bittlinger G, Powell CF, Kastengren AL, Wang J (2007) X-Ray Measurements of the Mass Distribution in the Dense Primary Break-Up Region of the Spray from a Standard Multi-Hole Common-Rail Diesel Injection System. Proc. 21st ILASS (Europe).
- Linne M, Paciaroni M, Hall T, Parker T (2006) Ballistic imaging of the near field in a diesel spray. Exp. Fluids 40: 836-846.
- Naber J, Siebers DL (1996) Effects of gas density and vaporisation on penetration and dispersion of Diesel sprays. SAE Paper 960034.
- Payri F, Bermúdez V, Payri R, Salvador FJ (2004) The influence of cavitation on the internal flow and the Spray characteristics in diesel injection nozzles. Fuel 83: 419-431.

Payri R, García JM, Salvador FJ, Gimeno J (2005) Using spray momentum flux measurements to understand the influence of Diesel nozzle geometry on spray characteristics. *Fuel* 84: 551-561.

Payri R, Tormos B, Salvador FJ, Araneo L (2008) Spray droplet velocity characterization for convergent nozzles with three different diameters. *Fuel* 87: 3176- 3182.

Post S, Iyer V, Abraham J (2000) A study of near-field entrainment in gas jets and sprays under diesel conditions. *ASME J. Fluids Eng.* 122: 385-395.

Prasad CMV, Kar S (1976) An investigation on the diffusion of momentum and mass of fuel in a Diesel fuel spray. *ASME J. Eng. Power* 76-DGP-1: 1-11.

Ramirez AI, Som S, Aggarwal SK, Kastengren AL, El-Hannouny EM, Longman DE, Powell CF (2009) Quantitative X-ray measurements of high-pressure fuel sprays from a production heavy duty diesel injector, *Exp. Fluids* 47:119–134

Rajaratnam N (1976) *Turbulent jets*. Elsevier Scientific Publishing Company.

Reitz RD, Bracco FV (1982) Mechanism of atomisation of a liquid jet. *Phys. Fluids* 25 (10): 1730-1742.

Ricou FP, Spalding DB (1961) Measurements of entrainment by axisymmetrical turbulent jets. *J. Fluid Mech.* 11: 21-32.

Rife J, Heywood JB (1974) Photographic and performance studies of Diesel combustion with a rapid compression machine. *SAE Paper* 740948.

Roisman IV, Araneo L, Tropea C (2007) Effect of ambient pressure on penetration of a diesel spray. *Int. J. Multiphase Flow* 33 (8): 904-920.

Roisman IV, Tropea C (2001) Flux measurements in sprays using phase doppler techniques. *Atomization spray* 11: 667-699.

Saliba R, Baz I, Champoussin JC, Lance M, Marié JL (2004) Cavitation effect on the near nozzle spray development in high-pressure diesel injection. *Proc. 19th ILASS (Europe)*.

Schlichting H (1978) *Boundary layer theory*. McGraw-Hill.

Sinnamon JF, Lancaster DR, Stienen JC (1980) An experimental and analytical study of engine fuel spray trajectories. *SAE Paper* 800135.

Spalding DB (1979) *Combustion and mass transfer*. Pergamon press.

Sou A, Hosokawa S, Tomiyama A (2007) Effects of cavitation in a nozzle on liquid jet atomization. *Int. J. Heat Mass Tran.* 50 (17-18): 3575-3582.

Subramaniam S (2001) Statistical modelling of a spray as using the droplet distribution function. *Phys. Fluids* 13 (3): 624-642.

Tanner FX, Feigl A, Ciatti SA, Powell CF, Cheong S-K, Liu J, Wang J (2006) Structure of high-velocity dense sprays in the near-nozzle region. *Atomization Spray* 16: 579-597.

Way RJB (1977) Investigation of interaction between swirl and jets in direct injection Diesel engines using a water model. *SAE Paper* 770412.

Wu KJ, Reitz RD, Bracco FV (1986) Measurements of drop size at the spray edge near the nozzle in atomising liquid jets. *Phys. Fluids* 29 (4): 941-951.

Wu KJ, Santavicca DA, Bracco FV (1984) LDV measurements of drop velocity in Diesel-type sprays. *AAIA J.* 22 (9): 1263-1270.

Yue Y, Powell CF, Poola R, Wang J, Schaller JK (2001). Quantitative measurements of diesel fuel spray characteristics in the near-nozzle region using X-ray absorption. *Atomization Spray* 11 (4): 471-490.

## FIGURE CAPTIONS

Figure 1. Initial and Main Region in a jet.

Figure 2a. Experimental velocity profiles adimensionalized in different sections of the spray. Comparison with Gaussian profiles.

Figure 2b. Velocity in the spray's axis. Comparison of experimental and theoretical results.

Figure 3.a. Scheme of x-ray measuring technique.

Figure 3.b. Description of integration for calculating  $M'$ .

Figure 4.a,b. Summary of experimental conditions and measuring positions in the x-ray tests.

Figure 4.c,d. X-ray experimental data from radial measurements.

Figure 5: Numerical procedure for evaluating  $\theta_m$  and  $C_{axis}$  from x-ray measurements.

Figure 6: Evolution of the deviation between experimental and predicted  $M'$  in terms of  $\theta_m$  and  $C_{axis}$ .

Figure 7: Experimental vs. predicted  $M'$  radial profiles.

Figure 8.a: Comparison of experimental and predicted axial evolution of  $M'$ .

Figure 8.b: Axial concentration values resulting from the  $M'$  calculation process.

Figure 9: Comparison of axial concentration obtained from experimental results and model predictions for different Schmidt numbers.

Figure 10: Local velocity and concentration contour maps for Test 1 and Test 2 conditions.

Figure 11: Comparison of different radial profiles available in the literature.

## TABLES

Table 1: Summary of results from  $M'$  radial profiles optimization process

	<b>Test 1</b>	<b>Test 2</b>
<b>Axial position (mm)</b>	4	10
<b>Chamber density (kg/m<sup>3</sup>)</b>	21.7	5.65
<b>Axial concentration</b>	0.933	0.954
<b>Mass angle (°)</b>	20.25	14
<b>Average deviation (kg/m<sup>2</sup>)</b>	0.0021	0.0026



Table 2: Expressions for radial profiles in the literature

<b>Reference</b>	<b>Expression</b>
<b>Gaussian fit (current study)</b>	$U(x, r) = U_{axis}(x) \exp\left(-\alpha \left(\frac{r}{R}\right)^2\right)$
<b>Sinnamon <i>et al.</i> 1980</b>	$U(x, r) = U_{axis}(x) \left(1 - \left(\frac{r}{R}\right)^{1.5}\right)^2$
<b>Schlichting 1978</b>	$U(x, r) = U_{axis}(x) \left(1 - 0.293 \left(\frac{r}{r_{1/2}}\right)^{1.5}\right)^2$
<b>Spalding 1979</b>	$U(x, r) = U_{axis}(x) \left(1 + 0.414 \left(\frac{r}{r_{1/2}}\right)^2\right)^{-2}$

# FIGURES

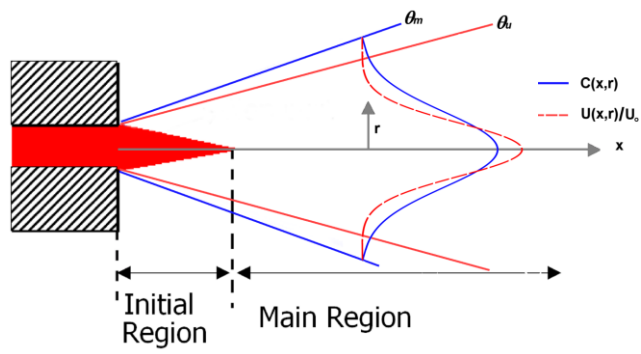


Figure 1. Initial and Main Region in a jet.

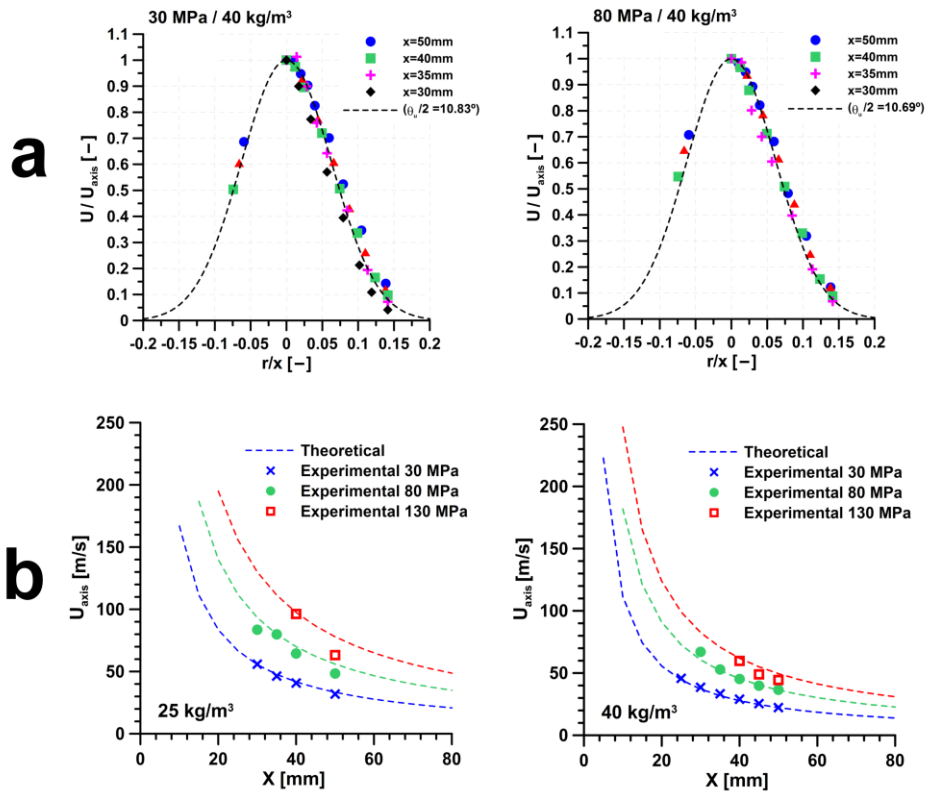


Figure 2a. Experimental velocity profiles adimensionalized in different sections of the spray. Comparison with Gaussian profiles.

Figure 2b. Velocity in the spray's axis. Comparison of experimental and theoretical results.

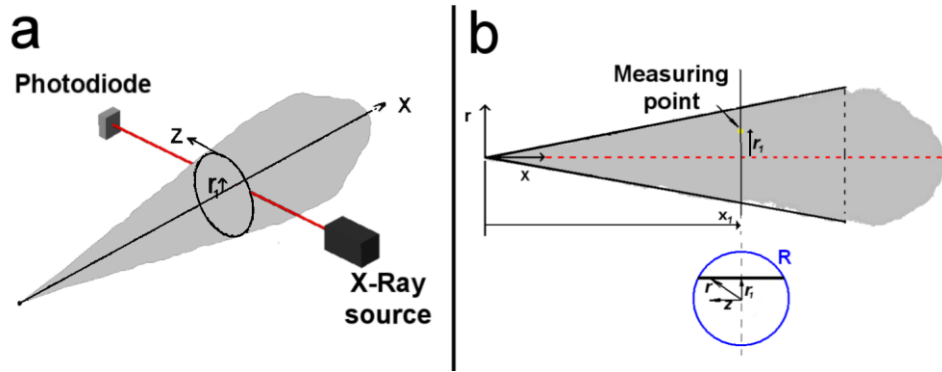


Figure 3.a. Scheme of x-ray measuring technique.

Figure 3.b. Description of integration for calculating  $M'$ .

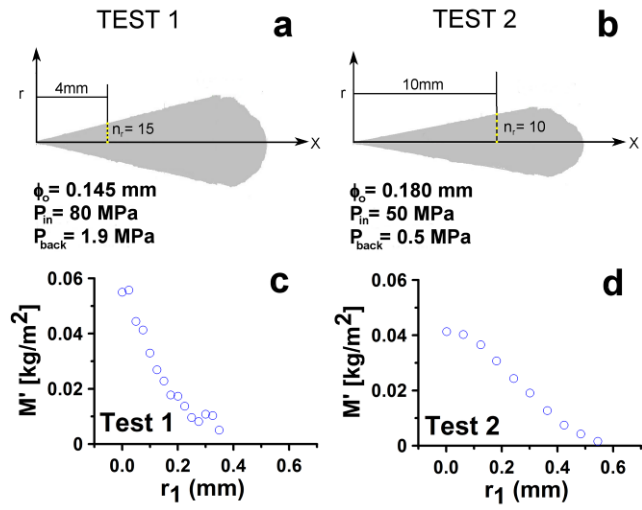


Figure 4.a,b. Summary of experimental conditions and measuring positions in the x-ray tests.

Figure 4.c,d. X-ray experimental data from radial measurements.

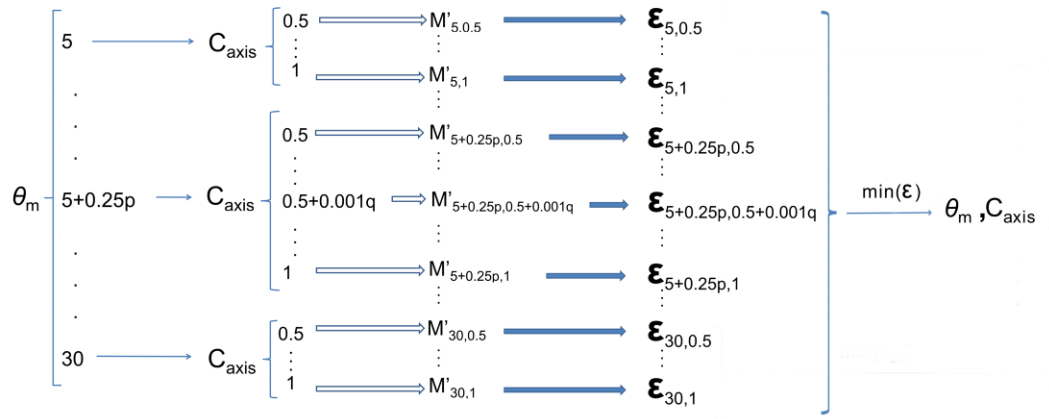


Figure 5: Numerical procedure for evaluating  $\theta_m$  and  $C_{axis}$  from x-ray measurements.

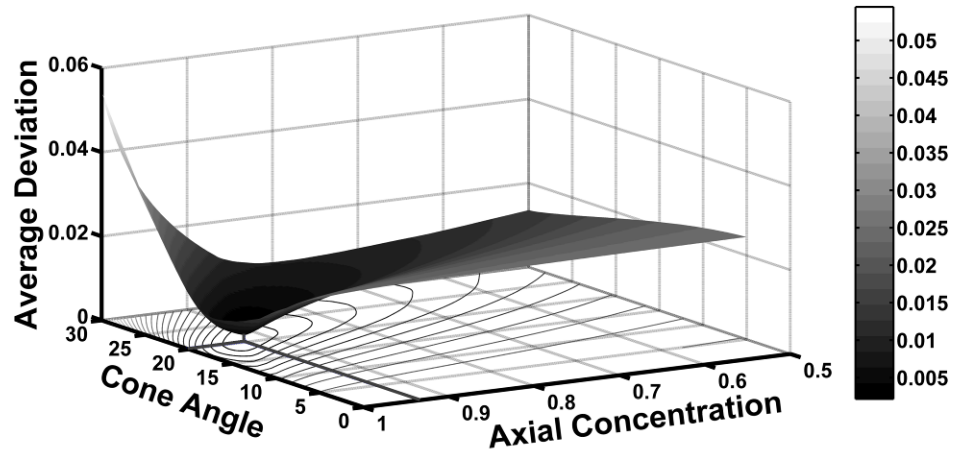


Figure 6: Evolution of the deviation between experimental and predicted  $M'$  in terms of  $\theta_m$  and  $C_{axis}$ .

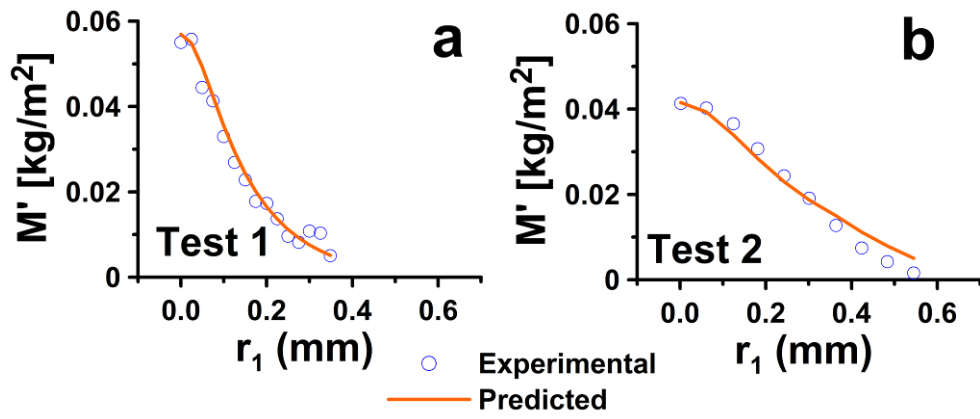


Figure 7: Experimental vs. predicted  $M'$  radial profiles.



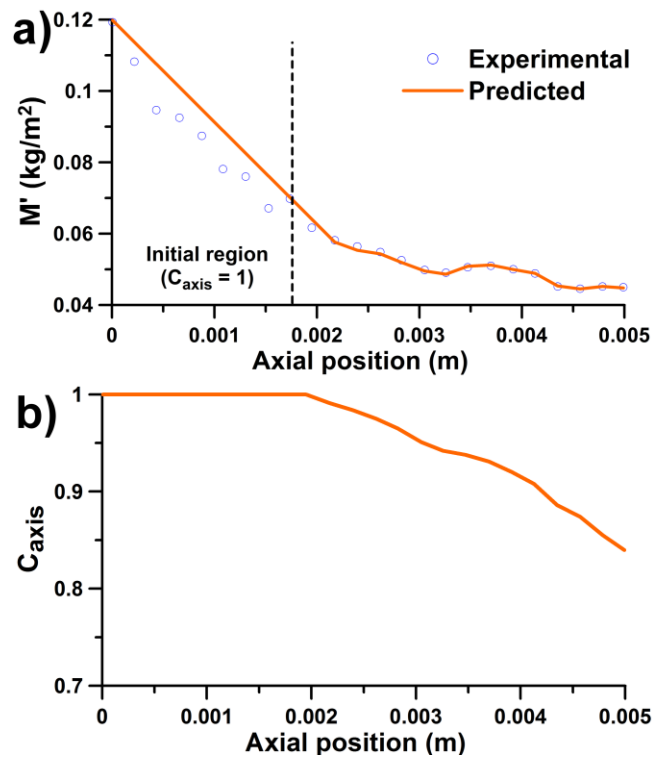


Figure 8.a: Comparison of experimental and predicted axial evolution of  $M'$ .

Figure 8.b: Axial concentration values resulting from the  $M'$  calculation process.

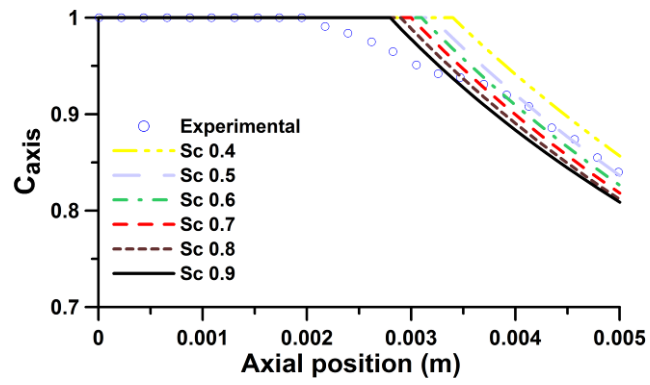


Figure 9: Comparison of axial concentration obtained from experimental results and model predictions for different Schmidt numbers.

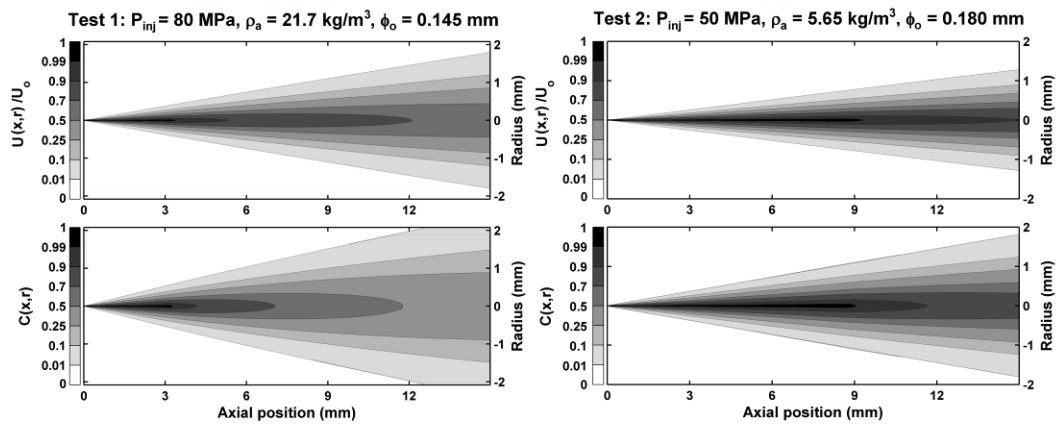


Figure 10: Local velocity and concentration contour maps for Test 1 and Test 2 conditions.

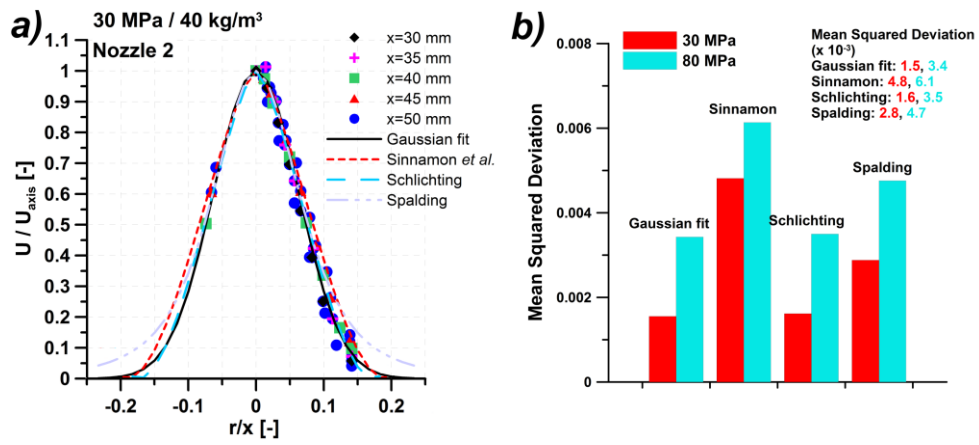


Figure 11: Comparison of different radial profiles available in the literature.